Analysis of the Surface Chemical Structure of Copolymers of Poly(sebacic anhydride) with Ricinoleic Acid Maleate Using XPS and ToF−SIMS

S. R. Leadley,*,†,‡ M. C. Davies,† A. Domb,§ R. Nudelman,§ A. J. Paul,|| and G. Beamson⊥

Laboratory of Biophysics and Surface Analysis, Department of Pharmaceutical Sciences, The University of Nottingham, Nottingham NG7 2RD, U.K. The School of Pharmacy, Department of Pharmaceutical Chemistry, The Hebrew University Jerusalem, Jerusalem, Israel 91120, CSMA Ltd., Armstrong House, Oxford Road, Manchester, M1 7ED, U.K., and RUSTI, Daresbury Laboratory, Warrington, Cheshire, WA4 4AD, U.K.

Received July 8, 1996; Revised Manuscript Received October 31, 1997

ABSTRACT: X-ray photoelectron spectrocopy (XPS) and time-of-flight secondary ion mass spectrometry (ToF−SIMS) have been used to characterize the surface chemistry of copolymers of poly(sebacic anhydride) with ricinoleic acid maleate. ToF−SIMS analysis yielded fragmentation patterns consisting of ions diagnostic of both monomers. Across the copolymer series, relative peak intensities of these diagnostic ions showed a good comparison between surface and bulk composition, in accordance with the XPS analysis. ToF−SIMS data also indicated that these copolymers consisted of either random or block sections.

Introduction

The first aromatic and aliphatic polyanhydrides were synthesized by Bucher and Slade in 1909[1] and Hill and Carothers in 1932,[2] respectively, as substitutes for polyesters in the textile industry. However, due to the hydrolytic instability of the anhydride linkage, they were found to be unsuitable for textile applications. This hydrolytic instability of the anhydride linkage, degrading the monomer units into dicarboxylic acids, has allowed the polyanhydrides to be exploited as a biodegradable polymer for biomedical applications.[3] High molecular weight polyanhydrides were successfully prepared by Domb and Langer in 1987, through a systematic study to determine the polymerization mechanism and factors affecting polymeric weight.[4] The authors have shown that the degradation rates of polyanhydrides can be manipulated through the choice of monomer, its hydrophobicity, and the number of multiple monomers in the copolymerization reaction.[5] The polyanhydrides have proved to be biocompatible, with the degradation byproducts producing no mutagenicity or cytoxicity.[6] Largely through the work of Langer and co-workers, this class of polymers have been used extensively in the design of novel drug delivery systems.[5,7−11]

In this study, we examine the surface chemistry of a new range of copolyanhydrides prepared from sebacic acid (SA) and ricinoleic acid maleate (RAM) which are potential materials for drug delivery systems, of the following structure:

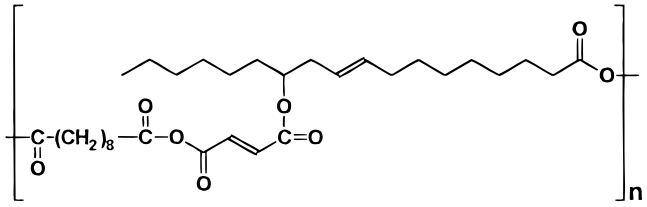

The surface chemistry of biodegradable polymers will play a major role in defining the nature and extent of the hydrolysis within the interfacial erosion region. In an attempt to define the surface chemical composition of such biodegradable systems, we have employed ToF−SIMS and XPS as complementary techniques providing detailed semiquantitative molecular information and quantitative elemental and chemical state information, respectively.[12−19] These studies have included reports on the interfacial chemistry of biodegradable homopolymers and copolymer series from the polyester,[15,16] poly(ortho ester),[17] polyanhydride,[18] and methacrylate[19] classes of polymer. One of the homopolymers under investigation in the previous study[18] was poly(sebacic anhydride). It is hoped that this study will show that ToF−SIMS and XPS can successfully be used to gain an insight into the surface character of the p(SA:RAM) copolymers listed in Table 1.

Materials and Methods

Polymer Synthesis. The PSA homopolymer and its copolymers with RAM were prepared by catalyzed melt−polycondensation of mixed anhydrides of sebacic acid and ricinoleic acid maleate in acetic acid, by the method described elsewhere.[4]

Instrumental Methods. XPS Analysis. XPS spectra were acquired using a Scienta ESCA300 spectrometer. This combines a high power (maximum 8 kW) rotating anode and monochromatized X-ray source (Al Kα), with high transmission electron optics and a multichannel detector. The design and the performance of the spectrometer have been described in

† The University of Nottingham.
‡ Current address: Dow Corning Ltd., Cardiff Road, Barry, Vale of Glamorgan, CF63 2YL, U.K.
§ The Hebrew University Jerusalem.
|| CSMA Ltd.
⊥ Daresbury Laboratory.

10.1021/ma960981t CCC: $15.00
Published on Web 11/12/1998

Table 1. Theoretical and Experimental Atomic Percentages for Polymers A to F

polymer	abbr	copolymer ratio SA	copolymer ratio RAM	atomic percentages theor % C	atomic percentages theor % O	atomic percentages exptl % C	atomic percentages exptl % O
poly[(sebacic anhydride)]	A	100		76.9	23.1	79.2	20.8
poly[(sebacic anhydride)-*co*-ricinoleic acid maleate)]	B	90	10	77.8	22.2	80.7	19.3
poly[(sebacic anhydride)-*co*-ricinoleic acid maleate)]	C	80	20	78.5	21.5	80.6	19.4
poly[(sebacic anhydride)-*co*-ricinoleic acid maleate)]	D	70	30	79.1	20.9	81.5	18.5
poly[(sebacic anhydride)-*co*-ricinoleic acid maleate)]	E	60	40	79.6	20.4	83.1	16.9
poly[(sebacic anhydride)-*co*-ricinoleic acid maleate)]	F	50	50	80.0	20.0	83.9	16.1

Table 2. Theoretical and Experimental Area Percentages of C 1s Components for Polymers A and F

peak type	peak no.	position (eV)	fwhm (eV)	% area under C 1s peak theory	% area under C 1s peak exptl	relative binding energy vs C^1−C/C^1−H (eV)
			polymer A			
C^1−C/C^1−H	1	285.00	0.97	60.0	63.7	
C^2−CO_2	2	285.65	0.95	20.0	17.4	0.65
C^3−O	3					
	4	287.84	1.20		1.0	2.84
C^5−O_2	5	289.49	1.02	20.0	17.4	4.49
			Polymer F			
C^1−C/C^1−H	1	285.00	1.04	65.6	72.5	
C^2−CO_2	2	285.68	0.90	15.6	11.1	0.68
C^3−O	3	286.57	1.21	3.1	4.5	1.57
	4	288.17	1.30		0.8	3.17
C^5−O_2	5	289.49	1.11	15.6	11.1	4.49

detail elsewhere.[20,21] Spectra were recorded at 150 eV pass energy, 0.5 mm slit width, 2.8 kW X-ray source power, and a takeoff angle of 45°. Charge compensation was achieved using a thermionic emission electron flood gun. The electron energy was 2−3 eV, and optimum spectral resolution was obtained with the sample at 90° to the flood gun beam corresponding to an electron takeoff angle of 45°. After peak fitting the C 1s envelope, all spectra were shifted so that the unfunctionalized aliphatic C 1s component occurs at 285 eV binding energy.

The surface atomic compositions were calculated from core line areas (using a straight line background) divided by the appropriate sensitivity factors. These factors were determined experimentally from clean polymers of known composition (poly(ethylene terephthalate) and nylon 6,6). Curve fitting of the C 1s envelope was performed using the Scienta ESCA300 data system software. This describes each of the components of a complex envelope as a Gauss-Lorentzian sum function.[22]

ToF−SIMS Analysis. ToF−SIMS analysis was performed using a VG Ionex IX23S instrument based on the Poschenrieder design, which has been described in detail elswhere.[23] A 30 keV Ga^+ primary ion beam was used at an incident angle of 38° to surface normal. The secondary ions were accelerated to ±5 keV for the analysis by applying a bias to the sample. For each sample, both positive and negative secondary ion spectra were collected using a total primary ion dose of 2×10^{11} ions cm^{-2}. Such a dose lies well below the damage threshold value of 1×10^{13} ions cm^{-2} for static SIMS.[24] A DEC PDP 11 computer system was used for spectral acquisition, storage, and data processing. Charge compensation was achieved using a pulsed low-energy electron source.

Sample Preparation. Samples were prepared for XPS analysis as thin films on glass by spin casting from 1 to 2% w/w solution in chloroform (HPLC grade, Fisons). A 13 mm diameter glass microscope coverslip was cleaned with tissue and 2-propanol, and mounted on a sample stub with double-sided tape. Samples were prepared for ToF−SIMS analysis as thin films on aluminum foil from 0.5 w/v% solution in chloroform (HPLC grade, Fisons).

Results and Discussion

XPS Analysis. The XPS analysis of PSA and its copolymers detected only carbon and oxygen in their survey scans. The lack of signal arising from the underlying substrate in the wide scans of all the polymers indicated the lack of elemental contamination and continuity of the polymer films. The experimental and theoretical atomic percentages for the PSA homo- and copolymers are shown in Table 2. It can be seen that the experimental carbon composition was slightly higher than expected from the theoretical stoichiometry for all the polymers (2−4%). This could be representative of adventitious hydrocarbon contamination or possibly indicative of some form of photodegradation during analysis. Despite the markedly different molecular structure of the homopolymers, there was only a very small difference in the surface composition across the range of these copolymers. However, despite these anticipated subtle differences in atomic composition of the copolymer series of polymers A to F (not shown), the expected increase in carbon levels associated with the increasing bulk of ricinoleic acid maleate (RAM) was observed. This increase in percentage carbon composition was complemented within the valence band spectra of polymers A to F, with a decrease in the intensity of the O 2s signal relative to the C 2s signal as the proportion of RAM increased.

The high-resolution C 1s spectra for polymers A and F are shown in Figures 1a and 1b, respectively. Components associated with the aliphatic carbon (C^1−C/C^1−H), the aliphatic carbon attached to the anhydride group (C^2−CO_2), and the carbon within the anhydride group (C^5−O_2), were included for all the poly(anhydride) C 1s spectra. An additional component corresponding to the ester linkage to the maleate within RAM (C^3−O) was also inserted in the copolymer C 1s spectra. The intensity of peak 3 was found to increase as the proportion of RAM within the copolymer series. The curve fitting procedure involved the fixing of the relative areas of peaks 2 and 5 in a 1:1 ratio, in accordance with their theoretical stoichiometry. The fitting procedure of this series of polymers also required the inclusion of an additional component (peak 4), indicating the presence of an impurity or degradation product.

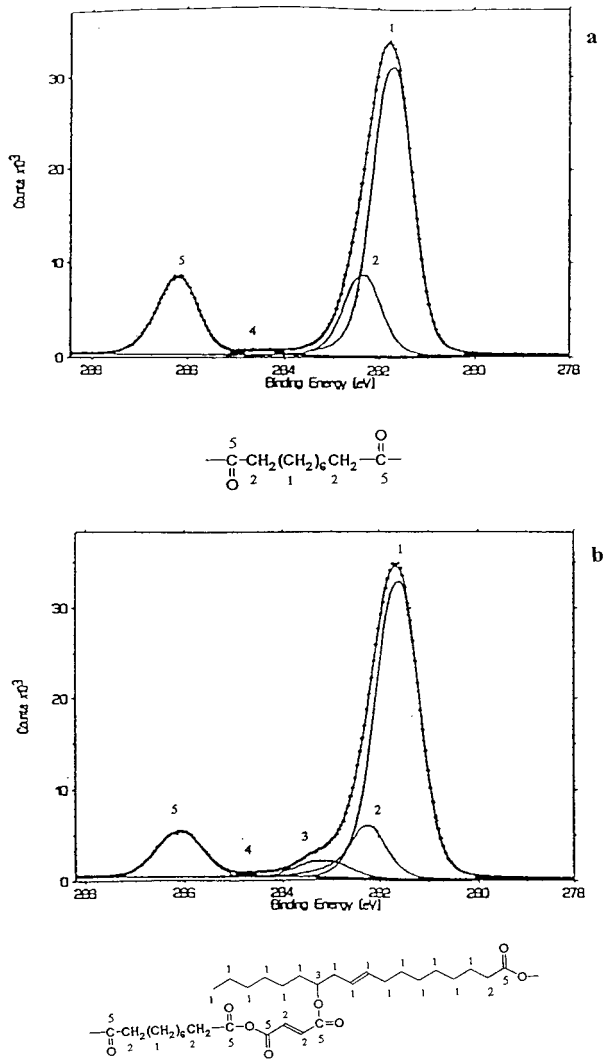

Figure 1. (a) C 1s XPS spectrum of polymer A. (b) C 1s XPS spectrum of polymer F.

The binding energies, fwhm, and theoretical and experimental area percentages for the components of the C 1s spectra of the polymers A and F are shown in Table 2. The effect of charging in the recorded spectra was corrected by referencing C^1−C/C^1−H to 285.0 eV. The binding energies of peaks 2 and 5 were consistent in both polymers at 285.7 and 289.5 eV, respectively, which was in accord with binding energies in the C 1s envelope in a previous XPS study of polyanhydrides.[18] In both cases, it can be seen that the experimental area percentage of the carbon component C^1−C/C^1−H was higher than the theoretical value, which may have been due to some form of hydrocarbon contamination. However, it can be seen that the experimental area percentage of the C^1−C/C^1−H component of the PSA homopolymer (polymer A) was 3.7% higher than expected, whereas the experimental area percentage of the C^1−C/C^1−H component of polymer F was 6.9% higher than expected, suggesting that some form of surface segregation of the RAM component occurs in polymer F.

The binding energy of peak 3 in the C 1s spectrum of polymer F was at 286.6 eV, being consistent with C 1s spectra of other polymers with ester linkages, as described elsewhere.[25] It should be noted that the theoretical ratio of peak 3 to peaks 2 and 5 was 0.2; however, the experimental ratio in polymer F was found to be

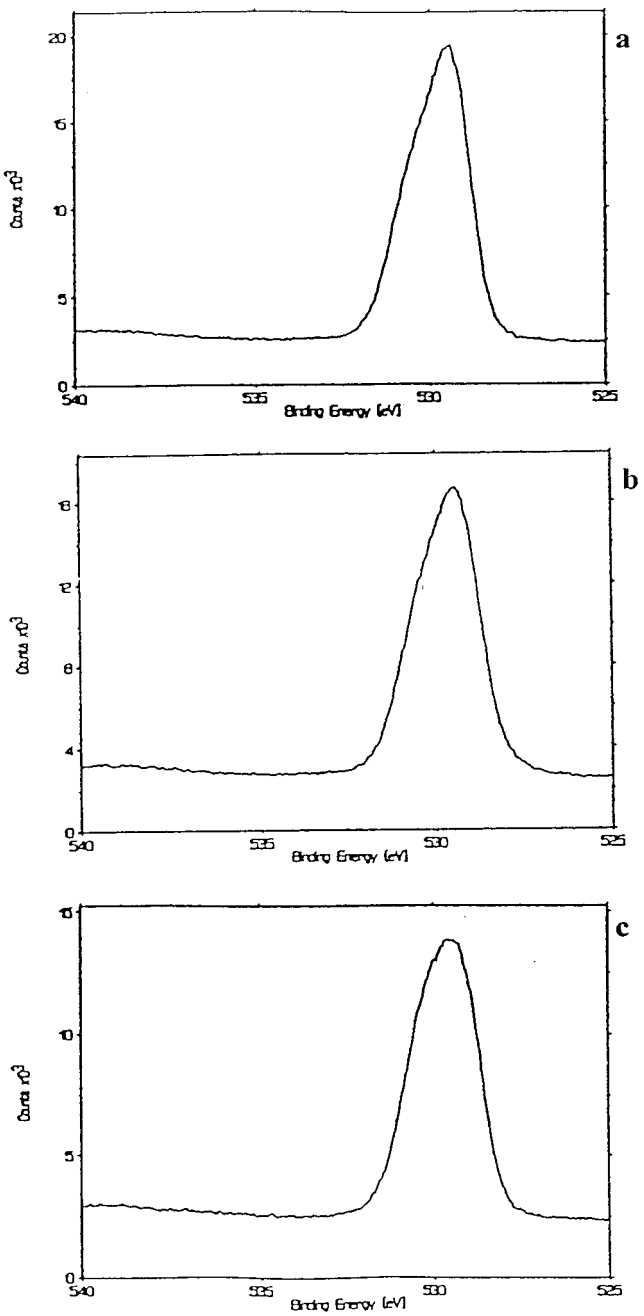

Figure 2. (a) O 1s XPS spectrum of polymer A. (b) O 1s XPS spectrum of polymer C. (c) The O 1s XPS spectrum of polymer F.

0.4, (see Table 2). This could possibly be due to some form of surface segregation of the RAM component of the copolymers, which is in accord with the increased C^1−C/C^1−H component of polymer F.

The O 1s spectra for polymers A to F showed a change in shape from asymmetric to symmetric as the proportion of RAM increased, as shown in Figure 2. This was as expected as an asymmetric O 1s spectrum is typical of polyanhydrides,[18] and as the proportion of RAM increased, the contribution from the ester component caused greater symmetry to be seen.

ToF−SIMS Analysis. ToF−SIMS spectra were acquired for all the polyanhydrides under investigation in both the negative ion and positive ion modes. For clarity, the negative and positive ion ToF−SIMS spectra will be discussed separately.

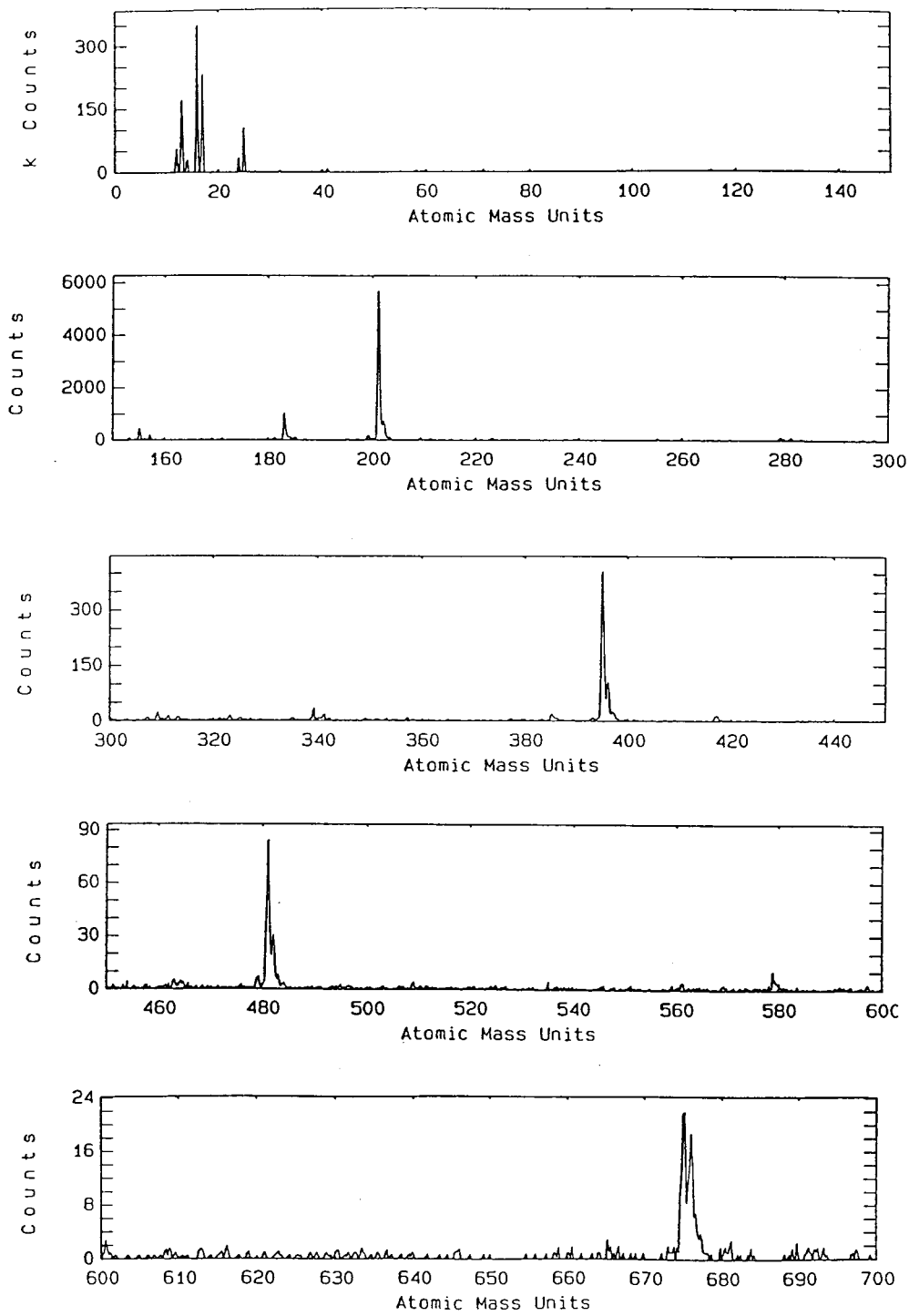

Figure 3. Negative ion ToF−SIMS spectrum of polymer C. *m/z* 0−700.

Negative Ion ToF−SIMS Spectra. The negative ion ToF−SIMS spectrum of the copolymer C in the mass region *m/z* 0−700 is typical of the range of polymers under investigation, as shown in Figure 3. It was observed that the homopolymer A and the copolymers B−F were similar in the mass region *m/z* 0−100. As is the case with many polymers containing oxygen, the most dominant ions in this region were at *m/z* 16 and 17, which can be assigned to O^- and HO^-, respectively. Other ions observed in this mass region include those at *m/z* 41 and 71, which can be assigned to $[C_2HO]^-$ and $[C_3H_3O_2]^-$, respectively.

The negative ion ToF−SIMS spectra of the polymers A, C, and F in the region *m/z* 100−220 are shown in Figure 4a−c. The negative ion ToF−SIMS spectrum of the PSA homopolymer (polymer A) was the same as that described previously,[18] with diagnostic ions being observed at *m/z* 113, 127, 141, 155, 183, and 201, as shown in Figure 4a. The ions at *m/z* 183 and 201 can be assigned to $[M_{SA} - H]^-$ and $[M_{SA} + OH]^-$, respectively.

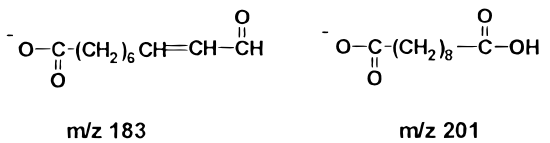

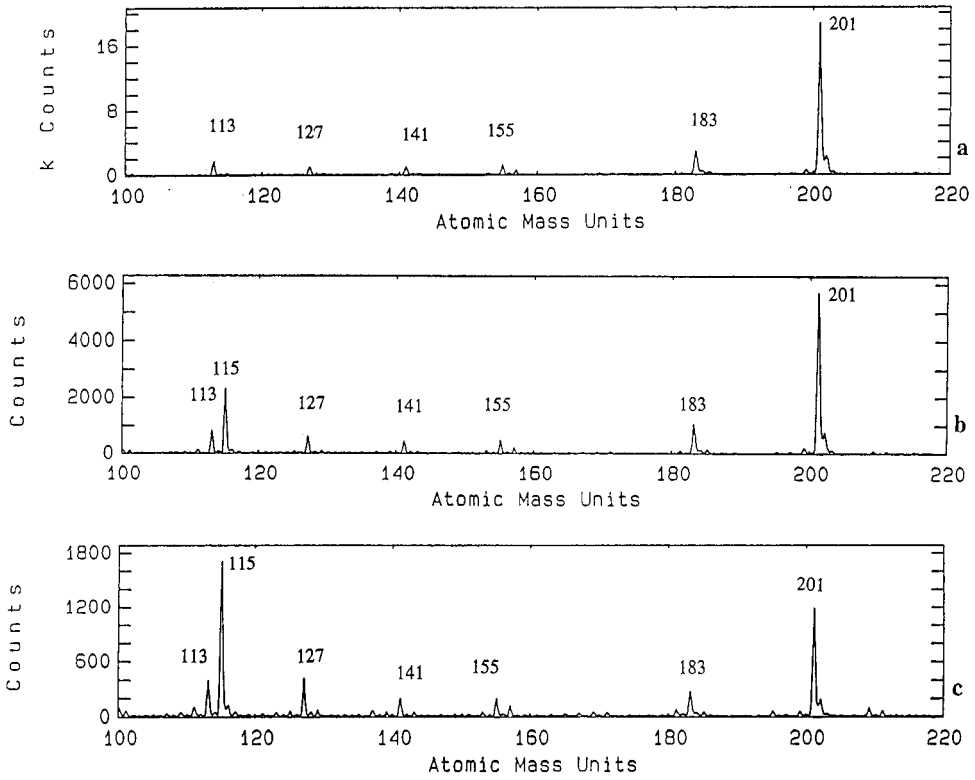

Figure 4. Negative ion ToF−SIMS spectra of (a) polymer A, (b) polymer C, and (c) polymer F. *m*/*z* 100−220.

Table 3. Anions Observed at > *m*/*z* 220 in the Negative Ion ToF−SIMS Spectra of Polymers A−F

	polymer					
anion	A	B	C	D	E	F
$[(M_{RAM} \pm H) - M_{mal}]^-$	279\81[a]	279\81	279\81	279\81	279\81	279\81
$[(M_{RAM} - M_{mal}) + O - H]^-$		295	295	295	295	295
$[(M_{RAM} - M_{mal}) + OH]^-$		297	297	297	297	297
$[2M_{SA} + OH]^-$	385	385				
$[(M_{RAM} + OH]^-$		395	395	395	395	395
$[M_{SA} + (M_{RAM} - M_{mal}) + OH]^-$		481	481	481	481	481
$[3M_{SA} + OH]^-$	569	569				
$[M_{RAM} + M_{SA} + OH]^-$		579	579	579		
$[M_{RAM} + (M_{RAM} - M_{mal}) + OH]^-$		675	675	675	675	675

[a] Very weak—attributed to a minor carboxylate impurity.

It can be seen from the negative ion ToF−SIMS spectra of the p(SA:RAM) copolymers (as shown in parts b and c of Figure 4), that an additional ion at *m*/*z* 115 was observed, which increased in relative ion intensity as the proportion of RAM in the copolymer increased. The ion at *m*/*z* 115 may be assigned to the pendant maleate group from the RAM component $[M_{mal} + OH]^-$ of the following structure:

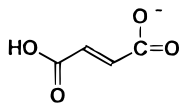

m/z 115

In contrast to the previous ToF−SIMS study of polyanhydrides,[18] detailed fragmentation patterns were observed in the negative ToF−SIMS spectrum of the homopolymer A and the copolymers B−F with anions of masses greater than *m*/*z* 220 as listed in Table 3. It can be seen that the PSA homopolymer yielded the ions $[2M_{SA} + OH]^-$ and $[3M_{SA} + OH]^-$ at *m*/*z* 385 and 569, respectively. It was also observed that the copolymers

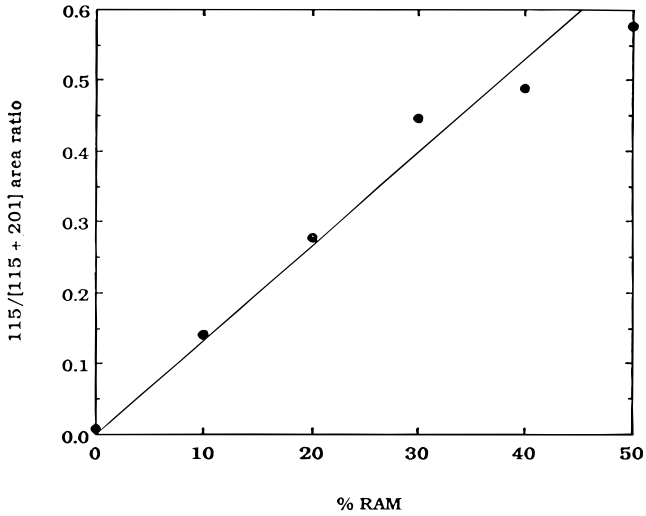

Figure 5. Plot of the peak area ratio for *m*/*z* 115 and *m*/*z* 201 (diagnostic of RAM and SA, respectively) vs the percent composition of the RAM monomer in the copolymer series.

B − F yielded the ion $[M_{RAM} + OH]^-$ at *m*/*z* 395, and an ion at *m*/*z* 279 which can be attributed to the RAM

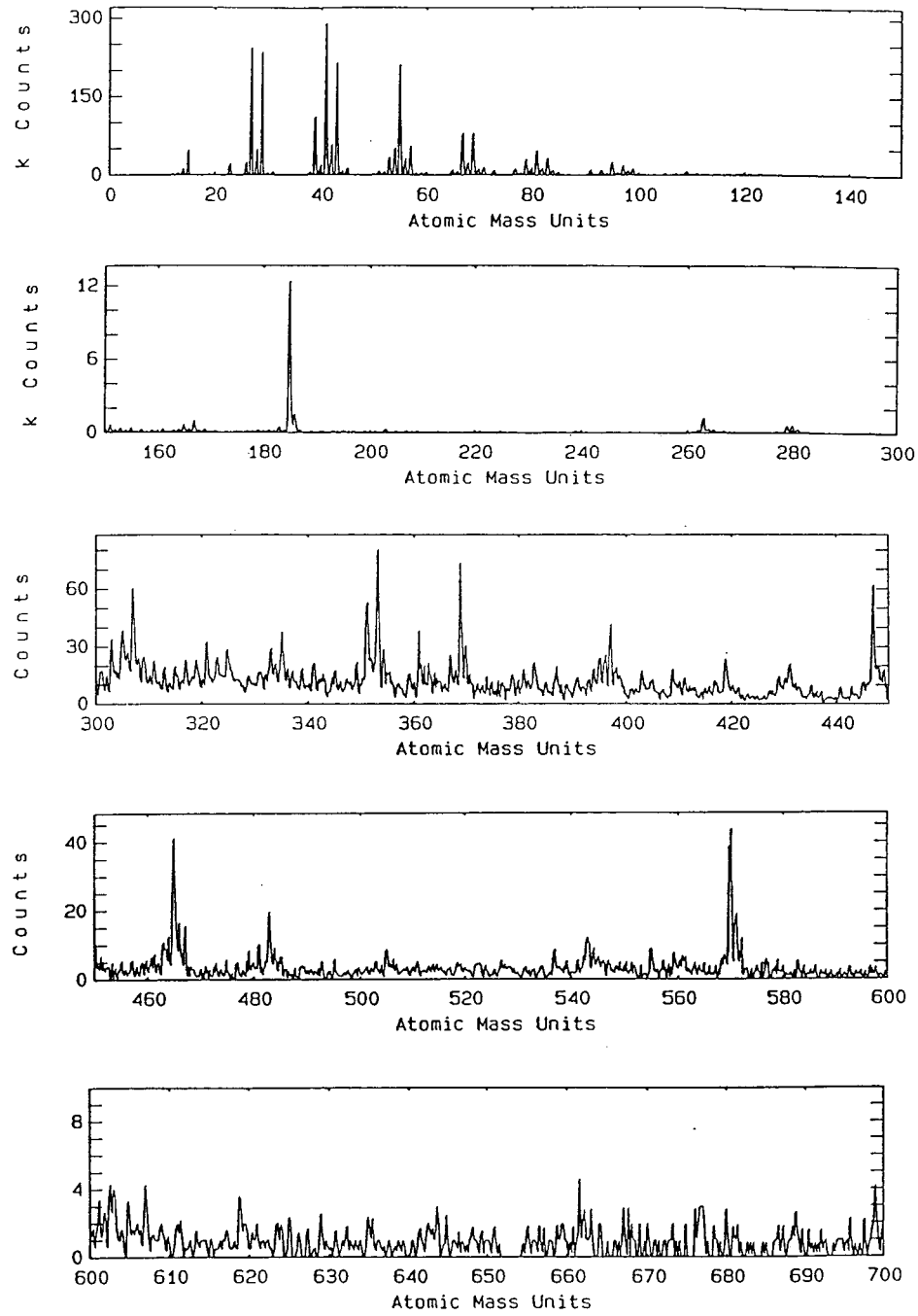

Figure 6. Positive ion ToF−SIMS spectrum of polymer C. *m/z* 0−700.

molecular ion minus the pendant maleate group M_{mal} and a proton $[M_{RAM} - M_{mal} - H]^-$, which could have the following structure:

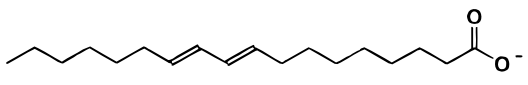

m/z 279

Ions were also observed in the negative ion ToF−SIMS spectra of the p(SA:RAM) copolymers (Polymers B − F) which can be attributed to the M_{SA} molecular ion attached to the M_{RAM} molecular ion and its fragments, as shown in Table 3. It can be seen that an ion at *m/z* 675 was observed in the negative ion spectra of the p(SA:RAM) copolymers, (polymers B−F), which has been attributed to $[M_{RAM} + (M_{RAM} - M_{mal}) + OH]^-$. This confirms that polymers B−F contain block sequences in the copolymers chain, which was supported by evidence of the $[nM_{SA} + OH]^-$ ions at *m/z* 385 and 569 being present in the negative ion ToF−SIMS spectrum of polymer B. However, ions were also observed in the negative ion ToF−SIMS spectra of p(SA:RAM) copolymers at *m/z* 481 and 579 attributed to $[M_{SA} + (M_{RAM} - M_{mal}) + OH]^-$ and $[M_{RAM} + M_{SA} + OH]^-$, respectively, indicating that a random sequence of the monomers was present. Therefore, the ToF−SIMS data provides evidence which suggests that the copolymers consist of either random or block sections in the polymer chain.

It is evident from Figure 4 that the relative intensities of the $[M_{mal} + OH]^-$ ion at *m/z* 115 and the $[M_{SA} + OH]^-$ ion at *m/z* 201 observed in the negative ion ToF−SIMS

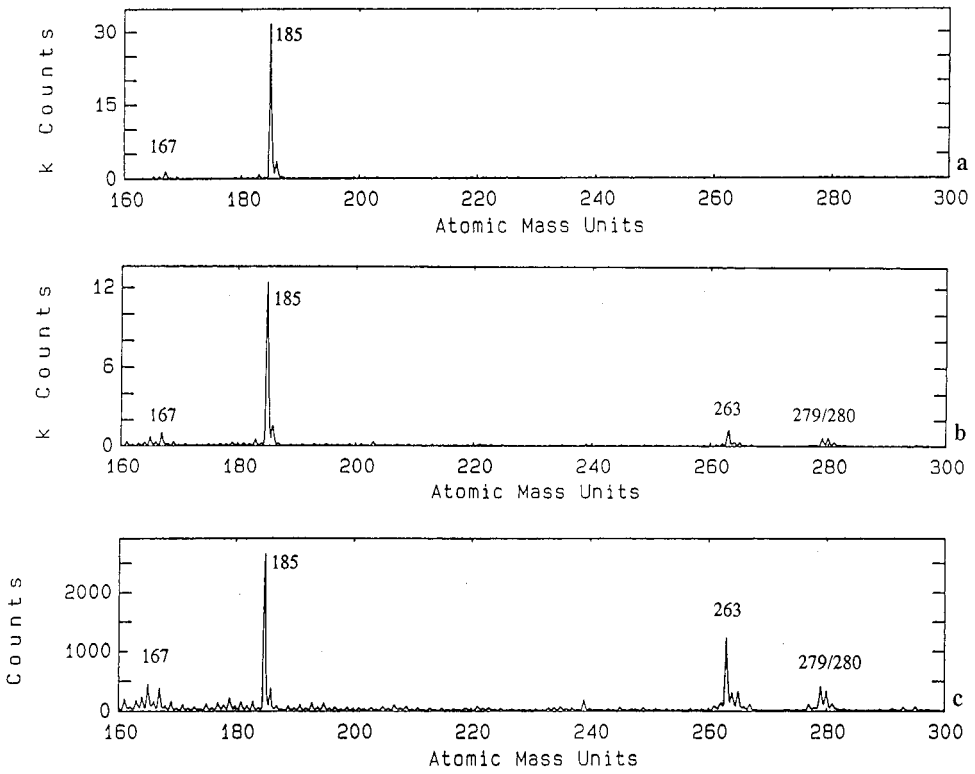

Figure 7. Positive ion ToF−SIMS spectra of (a) polymer A, (b) polymer C, and (c) polymer F. *m/z* 160−300.

spectra change with the bulk copolymer composition. These ions may be employed to compare their relative peak areas as a function of copolymer composition. Figure 5 shows the comparison of the peak area, *A*, of the *m/z* 115 (diagnostic of the RAM monomer) and the *m/z* 201 (diagnostic of SA monomer) peaks over the entire copolymer range. It can be seen that the $A_{115}/A_{115} + A_{201}$ ratio was fairly linear across the copolymer series with, perhaps, some deviation from linearity at a RAM content greater than 30%. This suggests that the diagnostic anions of the monomer components reflect the surface composition of the copolymer series as shown by the XPS analysis.

Positive Ion ToF−SIMS Spectra. The positive ion ToF−SIMS spectra of the copolymer C in the mass region *m/z* 0−700 is shown in Figure 6. It was observed that the homopolymer A and the copolymers B−F were similar in the mass region *m/z* 0−100. In this region, the dominant cations were observed at *m/z* 29, 55, 69, and 85, as described previously,[18] which can be attributed to hydrocarbon fragments C_nH_m+.[18]

The positive ion ToF−SIMS spectra of the polymers A, C, and F in the region *m/z* 160−300 are shown in Figure 7a−c, respectively. The PSA homopolymer (polymer A) positive ion ToF−SIMS spectrum was the same as that described previously,[18] with diagnostic ions being observed at *m/z* 167, and 185, as shown in Figure 7a. These diagnostic ions at *m/z* 167 and 185 can be assigned to $[M_{SA} - OH]^+$ and $[M_{SA} + H]^+$, respectively. It can be seen from the positive ion ToF−SIMS spectra of the p(SA:RAM) copolymers in parts b and c of Figure 7, that additional ions were observed at *m/z* 263, 279, and 280, which increased in relative ion intensity as the proportion of RAM in the copolymer increased. The ion at *m/z* 263 can be assigned to the RAM component minus the pendant maleate group (M_{mal}) and the loss of OH, $[(M_{RAM} - OH) - M_{mal}]^+$, of the following structure:

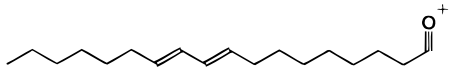

m/z 263

The ions at *m/z* 280 and 279 can be assigned to the radical cation of RAM minus the pendant maleate group $[(M_{RAM} - M_{mal}]^{+\cdot}$, and the *m/z* 263 ion plus oxygen $[M_{RAM} - M_{mal} - H]^+$, respectively, which could have the following structures:

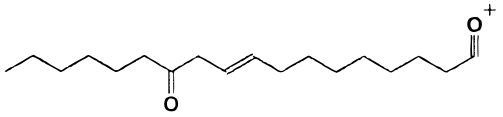

m/z 279

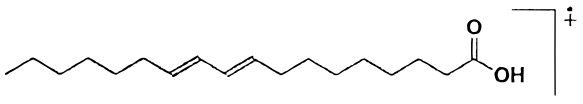

m/z 280

As observed in the negative ion ToF−SIMS spectra, detailed fragmentation patterns were observed, with cations of masses greater than *m/z* 300 in the positive ToF−SIMS spectrum of the homopolymer A and the copolymers B−F, as listed in Table 4. It can be seen that the PSA homopolymer, polymer A, yielded the ions $[nM_{SA} + H]^+$, where $n = 1$ and 2. There was also evidence which suggests that polymers B−F may con-

Table 4. Cations Observed at >*m/z* 300 in the Positive Ion ToF−SIMS Spectra of Polymers A−F

	polymer					
cation	A	B	C	D	E	F
$[2M_{SA} - O + H]^+$	353	353	353	353		
$[2M_{SA} + H]^+$	369	369	369	369		
$[(M_{RAM} + OH) + 2H]^+$		397	397	397	397	397
$[M_{SA} + (M_{RAM} - OH) - M_{mal}]^+$		447	447	447	447	447
$[M_{SA} + (M_{RAM} + H) - M_{mal}]^+$		465	465	465	465	465
$[3M_{SA} - O + H]^+$	537					
$[M_{SA} + (M_{RAM} - OH) - 2H]^+$		543	543	543	543	543

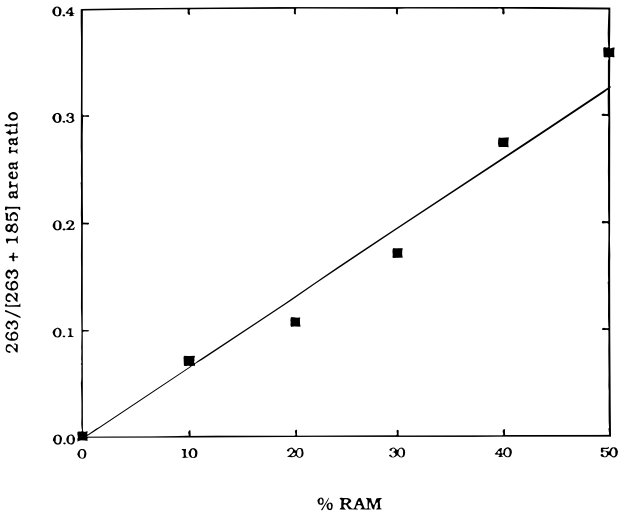

Figure 8. Plot of the peak area ratio for *m/z* 263 and *m/z* 185 (diagnostic of RAM and SA, respectively) vs the percent composition of the RAM monomer in the copolymer series.

tain block sequences in the copolymers chain, with the $[2M_{SA} + H]^+$ at *m/z* 369 being observed in the positive ion ToF−SIMS spectra of Polymers B, C and D. However, ions were also observed in the positive ion ToF−SIMS spectra of p(SA:RAM) copolymers at *m/z* 447, 465, and 543 attributed to $[M_{SA} + (M_{RAM} - OH) - M_{mal}]^+$, $[M_{SA} + (M_{RAM} + H) - M_{mal}]^+$, and $[M_{SA} + (M_{RAM} - OH) - 2H]^+$ indicating that a random sequence of the monomers was present. Therefore, the evidence agrees with that taken from the negative ion ToF−SIMS spectra, which suggests that the copolymers consist of either random or block sections in the polymer chain.

It is evident from Figure 7b,c that the relative intensities of the $[M_{SA} + H]^+$ ion at *m/z* 185 and the $[(M_{RAM} - OH) - M_{mal}]^+$ ion at *m/z* 263 change with the bulk copolymer composition. As shown for the negative ions at *m/z* 115 and 201 in the negative ion ToF−SIMS spectra, these ions may be employed to compare their relative peak areas as a function of copolymer composition. Figure 8 shows the comparison of the peak area, *A*, of the *m/z* 263 (diagnostic of the RAM monomer) and the *m/z* 185 (diagnostic of SA monomer) peaks over the entire copolymer range. It can be seen that the $A_{263}/A_{263} + A_{185}$ ratio was similar to the negative ion ratio $A_{115}/A_{115} + A_{201}$ shown in Figure 5, in that it was fairly linear across the copolymer series with, perhaps, some slight deviation from linearity at a RAM content greater than 30%. This suggests that the diagnostic cations of the monomer components reflect the surface composition of the copolymer series as shown by XPS analysis.

Conclusions

Both ToF−SIMS and XPS analyses have given a valuable insight into the surface chemical nature of these polyanhydride copolymers. The ToF−SIMS spectra of these materials displayed characteristic fragmentation patterns, which consisted of ions diagnostic of the polymers under investigation. The XPS data acquired from these polyanhydrides showed a good correlation between experimental composition and theoretical composition for the copolymers with a RAM content of up to 30%. The XPS data suggested that the copolymers with a RAM content greater than 30% exhibit a marginal surface enrichment of the RAM component. The modest higher surface level of RAM observed may be due to the copolymers with a RAM content greater than 30% having a higher degree of block structure than random monomer sequence. In good agreement with the XPS data, the diagnostic ions of the monomer components reflect the surface composition of the copolymer series. The ToF−SIMS data showed evidence suggesting that the copolymers consist of both random or block sections in the polymer chain. It was also shown that comparison of relative ion intensities in the ToF−SIMS spectra showed a fairly linear correlation between surface and bulk composition with, perhaps, some deviation from linearity at a RAM content greater than 30%. This modest surface enrichment of RAM when the copolymer concentration of RAM is greater than 30% may have an effect on the degradation of these polymers, which should be taken into account when using these copolymers for developing drug delivery systems.

References and Notes

(1) Bucher, J. E.; Slade, W. C. The anhydrides of isophthalic and terephthalic acids. *J. Am. Chem. Soc.* **1909**, *31*, 1319.

(2) Hill, J.; Carothers, W. H. Studies of polymerisation and ring formation. XIV. A linear superpolyanhydride and cyclic dimeric anhydride from sebacic acid *J. Am. Chem. Soc.* **1932**, *54*, 1569.

(3) Vert, M. Bioresorbable polymers for temporary therapeutic applications *Die Angew. Makromol. Chem.* **1989**, *166/167* 155.

(4) Domb, A. J.; Nudelman, R. Biodegradable polymers derived from natural fatty acids *J. Polym. Sci.* **1995**, *33*, 717.

(5) Leong, K. W.; Brott, B. C.; Langer, R. Bioerodible polyanhydrides as drug-carrier matrices 1: Characterisation, degradation, and release characteristics *J. Biomed. Mater. Res.* **1985**, *19*, 941.

(6) Leong, K. W.; D'Amore, P.; Marletta, M.; Langer, R. Bioerodible polyanhydrides as drug-carrier matrices 2: Biocompatibility and chemical reactivity *J. Biomed. Mater. Res.* **1986**, *20*, 51.

(7) Chasin, M.; Domb, A.; Ron, E.; Mathiowitz, E.; Langer, R.; Leong, K. W.; Lauencin, C.; Brem, H.; Grossman, S. In *Drugs and the pharmaceutical sciences*; Chasin, M., Langer, R., Eds.; Marcel Dekker: New York, 1990; Vol. 45, p 43.

(8) Rosen, H. B.; Chang, J.; Wnek, G. E.; Linhardt, R. J.; Langer, R. Bioerodible polyanhydrides for controlled drug delivery *Biomaterials* **1983**, *4*, 131.

(9) Leong, K. W.; Kost, J.; Mathiowitz, E.; Langer, R. Polyanhydrides for controlled release of bioactive agents *Biomaterials* **1986**, *7*, 364.

(10) Mathiowitz, E.; Langer, R. Polyanhydride microspheres as drug carriers 1. Hot melt microencapsulation *J. Control. Relat.* **1987**, *5*, 13.
(11) Mathiowitz, E.; Saltzman, M.; Domb, A.; Dor, P.; Langer, R. Polyanhydride microspheres as drug carriers II. Microencapsulation by solvent removal *J. Appl. Polym. Sci.* **1988**, *35*, 755.
(12) Hearn, M. J.; Ratner, B. D.; Briggs, D. SIMS and XPS studies of poly(urethane) surfaces. I. Preliminary studies *Macromolecules* **1988**, *21*, 2950.
(13) Davies, M. C.; Khan, M. A.; Short, R. D.; Akhtar, S.; Pouton, C.; Watts, J. F.; XPS and SSIMS analysis of the surface chemical structure of poly(caprolactone) and Poly(***β***-hydroxybutyrate-***β***-hydroxyvalerate) copolymers *Biomaterials* **1990**, *11*, 228.
(14) Brinen, J. S.; Greenhouse, S.; Jarrett, P. K. XPS and SIMS studies of biodegradable suture materials *Surf. Interface Anal.* **1991**, *17*, 259.
(15) Davies, M. C.; Short, R. D.; Khan, M. A.; Watts, J. F.; Brown, A.; Eccles, A. J.; Humphrey, P.; Vickerman, J. C.; Vert, M. An XPS and SIMS analysis of biodegradable biomedical polyesters *Surf. Interface Anal.* **1989**, *14*, 115.
(16) Leadley, S. R.; Davies, M. C.; Vert, M.; Braud, C.; Shard, A. G.; Paul, A. J.; Watts, J. F. Probing the surface chemical structure of the novel biodegradable polymer poly(*β*-malic acid) using ToF−SIMS and XPS. Manuscript in preparation.
(17) Davies, M. C.; Lynn, R. A. P.; Paul, A. J.; Vickerman, J. C.; Heller, J.; ToF−SIMS and XPS analysis of the surface chemical structure of some linear poly(ortho esters) *Macromolecules* **1991**, *24*, 5508.
(18) Davies, M. C.; Khan, M. A.; Domb, A.; Langer, R.; Watts, J. F.; Paul, A. J. The analysis of the surface chemical structure of biomedical aliphatic polyanhydrides using XPS and ToF-SIMS *J. Appl. Polym. Sci.* **1991**, *42*, 1597.
(19) Briggs, D.; Ratner, B. D. A semiquantitative SIMS analysis of the surfaces of random ethyl methacrylate: hydroxyethyl methacrylate copolyer films *Polym. Commun.* **1989**, *29*, 6.
(20) Gelius, U.; Wannberg, B.; Baltzer, P.; Fellner-Feldegg, H.; Carlsson, G.; Johansson, C.-G.; Larsson, J.; Munger, P.; Vegerfors, G. *J. Electron Spectrsco. Relat. Phenom.* **1990**, *52*, 747.
(21) Beamson, G.; Briggs, D.; Davies, S. F.; Fletcher, I. W.; Clark, D. T.; Howard, J.; Gelius, U.; Wannberg, B.; Baltzer, P. *Surf. Interface Anal.* **1990**, *15*, 541.
(22) *Scienta ESCA300 Users Manual.*
(23) Eccles, A. J.; Vickerman, J. C. *J. Vac. Sci. Technol.* **1989**, *A7*, 234.
(24) Briggs, D.; Hearn, M. J. Interaction of ion beams with polymer, with particular respect to SIMS *Vacuum* **1986**, *36*, 1005.
(25) Beamson, G.; Briggs, D. *High-resolution XPS of organic polymers−The Scienta ESCA300 database*; J. Wiley and Sons: Chichester, England 1992.

MA960981T